Iranian Journal of Chemical Engineering
Vol. 16, No. 2 (Spring 2019), IAChE

Interior Modification of Nano-Porous Fillers to Fabricate High-Performance Mixed Matrix Membranes

H. Sanaeepur [1,2*], A. Ebadi Amooghin [1,2], A. Kargari [3], M. Omidkhah [4], A. F. Ismail [5], S. Ramakrishna [6]

[1] Department of Chemical Engineering, Faculty of Engineering, Arak University, P. O. Box: 38156-8-8349, Arak, Iran
[2] Institute of Nanosciences & Nanotechnology, Arak University, Arak, Iran
[3] Membrane Processes Research Laboratory (MPRL), Department of Chemical Engineering, Amirkabir University of Technology (Tehran Polutechnic), Tehran, Iran
[4] Faculty of Chemical Engineering, Tarbiat Modares University, P. O. Box: 14115-143, Tehran, Iran
[5] Advanced Membrane Technology Research Centre (AMTEC), Faculty of Chemical and Energy Engineering, Universiti Teknologi Malaysia UTM, 81310 Johor Bahru, Johor, Malaysia
[6] Center for Nanofibers and Nanotechnology, Department of Mechanical Engineering, Faculty of Engineering, Engineering Drive, National University of Singapore, 117576, Singapore

ARTICLE INFO

Article history:
Received: 2018-10-08
Accepted: 2019-04-30

Keywords:
Ship-in-a-Bottle (SIB),
Macrocyclic Ag-Ligand Complex,
Nano-Porous Hybrid Filler,
Mixed Matrix Membrane,
Gas Separation

ABSTRACT

A new method is developed to enhance the gas separation properties of mixed matrix membranes (MMMs) by interior modification of an inorganic nano-porous particle. Ship-in-a-bottle (SIB), as a novel synthesis strategy, is considered to encapsulate a polyaza macrocyclic Ag-ligand complex into the zeolite Y, which has resulted in a new host-guest nano-composite. It is consequently incorporated into a glassy polymer matrix to fabricate a novel MMM for CO_2 separation. Accordingly, cellulose acetate (CA) with relatively low gas permeability is selected as the membrane polymeric matrix to provide an appropriate opportunity for better tracking the effect of incorporating the new synthesized nano-porous hybrids. The results showed a promising increase in both the CO_2 permeability (45.71 %) and CO_2/N_2 selectivity (40.28 %) of the prepared MMM over its pristine CA membrane. It can be concluded that the proposed method makes it possible to fabricate novel MMMs with significant intensification in the performance of the current MMMs.

1. Introduction

Hybrid metal oxides, which contain infinite metal-oxygen-metal arrays as a part of their structures, have developed in simultaneity with their analogues, metal-organic coordination polymers. Both are categorized conveniently into an important class of solids, the nano-porous hybrid materials [1-3]. Progress in the development of the hybrids concurrent with a conceptual approach of confining/replacement of the protein of natural enzymes by a size and shape of a selective

*Corresponding author: h-sanaeepur@araku.ac.ir

framework such as zeolites (which are capable to act as a protective environment and work collaboratively with the active sites in separation of species) has led to exploring a new class of host-guest nano-composites. Thoroughly, the "ship-in-a-bottle" (SIB) approach was first introduced to the field of synthesizing the zeolite catalysis [4]; the term illustrates the synthesis of hybrid nano-porous zeolites, which are formed by catalytic (guest) molecules encapsulated in the zeolite (host) cavities. A guest molecule (like a ship) is formed by assembling its separate constituent species in the zeolite cavities and has become larger than the pore aperture of the (bottle-like) zeolite. The guest nano-materials are confined and, yet, can freely move around within nano-scale domains of the host cavities and, hence, prevent leaching [5, 6].

In the past few decades, numerous host-guest hybrids consist of metal-ligand complexes confined within shells, or voids of the organic or inorganic "nano-containers" have been synthesized under different names of yolk-shell, core-shell, nanorattle, or ship-in-a-bottle nano-reactors and attracted more potential applications [7-9]. For example, Corma and Garcia [10] in a review article discussed the synthesis/characterization techniques necessary to study host-guest systems in zeolites prepared by SIB method and investigated the application of the systems as catalysts, photo-catalysts, sensors, molecular machines, etc. Liu et al. [11] provided an overview of advances in yolk-shell or rattle-typed nanostructures' synthesis and their potential applications in nano-reactors, biomedicine, and lithium-ion batteries. Fujie and Kitagawa [12] reviewed ionic liquids impregnated or encapsulated into the metal organic framework (MOF) porous supports so that they could be used in chemical reactions, extractions, catalysis, gas absorption, and electrolytes in electrochemical devices. More recently, Gkaniatsou et al. [13] developed an overview of enzyme-MOF biocomposites with MOFs as host platforms for bio-immobilization of the guest enzymes. Here, it is worth mentioning that the guest molecules included in the SIB synthesis are noted as "encapsulated" molecules to show their difference from "impregnated" molecules.

In comparison with zeolites and other common molecular sieves in which their pores are commonly capable to act as the non-selective ways that play an important role in the enhancement of permeability (not the selectivity), MOFs have attracted much attention concerning their role in gas separation mixed matrix membranes (MMMs) because: (i) the high surface area (3000-4500 m^2/g) and the controllable porosity [14], (ii) tendency towards the sorption of a specific gas, which facilitates gas separation from its mixture [15], (iii) organic linkages of MOFs are highly capable to functionalize, which results in adjusting necessary interactions required for adsorption; moreover, the size and available volumes of MOF's pores can be controlled through the size of the used functional group [16] and (iv) organic linkages of MOFs not only affect gas diffusion in MMMs, but also have effective interactions with polymeric membrane matrix, implying the compatibilizing effect [17-19]; the proper compatibilization can lead to an MMM without interfacial voids between polymer-particle [20, 21]. The last case is special due to the application of the MOFs to fabricating MMMs. However, some problems remain for the industrial use of the MOF-containing MMMs. In the case of other inorganic-organic compounds, MOFs include metal cations and/or cationic metal oxide clusters, which are

linked to organic molecules that will form a crystalline network. Thus, the MOFs called "coordination polymers"; as a coordination network, MOFs have lower mechanical stiffness and, thus, higher brittleness as compared to the zeolites. This higher flexibility of MOF backbones is accompanied by undesirable effects of breathing, gate opening, and linker dynamics [16] (for more information, see [22] and [23]). The so-called flexibility leads to lower CO_2/CH_4 selectivity of MOF membranes, compared to the zeolite ones [24]. In addition, it lowers the high-sorption selectivities of MOFs with the increasing pressure [25]. Even though the MOF-containing MMMs have mostly high thermal resistance, a high temperature in the membrane formation is highly required to overcome the severe interaction between MOF and their entrapped solvent molecules, leading to structural deformation upon solvent removal [26]. Flexibility of the metal-organic backbone of MOFs makes it easy to modulate them as a self-assembled membrane; however, the flexible structure of MOFs prevents an appropriate separation based on the penetrant sizes [16]. A method of synthesis of the continuous MOF crystal layers on porous inorganic/organic supports has been frequently applied in order to ensure the required mechanical stability of the thin film composites. However, the thin MOF films still deal with the lack of scalability in separating the gas species due to difficulties in the growth of a homogeneous, defect-free MOF crystal layer [27].

To overcome the discussed disadvantages of zeolites/MOFs (the two best adsorbents in the case of MMMs), the idea of combining all their advantages in one, encapsulating the proper metal-organic frameworks (i.e., metal-organic complexes) in the cages of zeolites comes to the fore so that a novel SIB-synthesized metal-organic filler can be tailored. As mentioned above, most of the studies on SIB approach have been devoted to creating a catalyst. On the other hand, due to the presence of many active sites in a catalyst, it can be used as a physic-chemical adsorbent. All adsorbents can be proposed as potential candidates to take part in MMMs. The SIB synthesized complexes have been mainly used as Schiff-base nano-catalysts due to the presence of organic ligands, which play the role of Lewis base (each organic ligand/atom is a Lewis base that donates one pair of valence electrons to the central acceptor/atom - as a Lewis acid - through a dative bond type association pathway) at the interactions with electron donor molecules serving as the Lewis acid [28]. In the case of CO_2 separation, not only the CO_2 diffusivity is essential, but also its proper solubility is of great importance in separation performance [29-31]. Appropriate intermolecular interactions between CO_2 molecules and membrane matrix similar to CO_2 condensability (the ratio of 2.73:1 was reported for CO_2 condensability compared to N_2 on the basis of Lennard–Jones well depth, ε/k (K)) in the membrane affect its solubility [30, 32-39].

In our previous work [40], we have studied the CO_2/CH_4 separation properties of Matrimid®5218-based MMMs containing zeolite Y encapsulated by a polyaza macrocyclic cobalt-ligand complex. The results revealed that both permeability and selectivity of the gases were extremely increased by the incorporation of the encapsulated fillers.

In this paper, a new potential application is introduced for encapsulated metal-ligand complexes in zeolites as the new fillers for mixed matrix polymeric gas separation

membranes. In this regard, a polyaza macrocyclic Ag-ligand complex is synthesized in a zeolite Y support through the SIB method to form a nano-porous hybrid solid, which will be embedded as a dispersed particle in a low permeable/moderate selective cellulose acetate (CA) polymeric membrane matrix. The relatively low permeability of CA matrix provides an appropriate opportunity for better tracking the effect of embedding the new synthesized nano-porous hybrids. Here, the fluctuations in gas permeation results of CA membranes observed by some authors [41-43] are entirely diminished by annealing the CA and CA-based MMMs. It should be noted that annealing resulted in somewhat lowering the permeability/selectivity of the CA membrane [39].

2. Experimental

2.1. Materials

Cellulose acetate (CA) (average Mn~ 30,000), acetyl content 39.8 wt %, and also sodium Y zeolite (NaY) powder (an average particle diameter of 1.22 μm) with Si/Al ratio of 2.53 were purchased from Sigma-Aldrich (Saint Louis, MO, USA). Tetrahydrofuran (THF), methanol, ethanol, 1,3-phenylenediamine, 2,4-pentanedione (or acetyl acetone), and silver nitrate were acquired from Merck Co. (Darmstadt, Germany) and used without further purification. High-quality distilled water (conductivity less than 2 μS/cm) was attained by a laboratory double distillation apparatus, GFL 2104 (Burgwedel, Germany). Carbon dioxide and nitrogen with 99.999 % purity were purchased from Technical Gases Ltd. supplied by Oxygen Yaran Company (Mahshahr, Iran).

2.2. Synthetic procedures

2.2.1. SIB synthesis

Part (1) Ion exchange: The ion exchange reaction was performed as described in detail by previous works [37, 38]. Briefly, prior to synthesis, the NaY powder was dried two days at 120 °C in a vacuum oven. 100 ml distilled water was poured into a 250 ml round glass bottle equipped with a plastic stopper (which, hereafter, is referred to as "reactor") and 100 mM silver nitrate salt was added and stirred for 1 h at 400 rpm to complete dissolution. Then, the white NaY powder was added at a ratio of 10 % (w/v) to the transparent colorless Ag^+ solution and was stirred rigorously for 24 h at 700 rpm and 90 °C. After completion of the ion exchange reaction between Ag^+ and Na^+ ions, a transparent suspension was obtained. Thereafter, the suspended solids were filtered and washed with hot distilled water repeatedly (5×20 ml) until clear wash water was obtained. It is worth noting that insufficient washing after ion exchange of NaY zeolite leads to partial blockage of the micro-pores by the adsorbed large cations or by the probable insoluble salt residues. It can be effective in the CO_2/N_2 selectivity considering the difficulty of gas diffusion into the blocked pores and/or the strong CO_2 adsorption by the ions/salts. The filtrate solution was analyzed by a Perkin-Elmer model AA300 (Perkin-Elmer Corp., Norwalk, CT) atomic absorption spectrophotometer (AAS), and a value of 94.62 % was found for the degree of ion exchange. Finally, the obtained solid was dried for two days at 120 °C in a vacuum oven. A dark white Ag(I)Na-Y powder, here named as Ag-1, was acquired after drying.

Part (2) Entrapping Ag^+-complexes into the zeolite cavities through the adsorption: Herein, 100 ml methanol was poured in the reactor, and the Ag-1 powder was added at a ratio of 10 % (w/v) and was stirred rigorously for 1 h at 700 rpm until a transparent

suspension was obtained. Then, 100 mM of a diamine, the flake-like 1,3-phenylenediamine, was added in the suspension and dissolved at 90 °C until its color changed to dark salmon at first and, after 48 h, with the complete formation of $[Ag(diamine)]^+$ complexes in the Ag-1 pores, became a dark gray suspension. Thereafter, the suspended solids were filtered and washed with ethanol repeatedly (5×20 ml). Next, the solids were dried overnight at 100 °C in an oven. Subsequently, the solids suspended at a ratio of 10 % (w/v) in a 100 mM aqueous sodium nitrate ($NaNO_3$) solution and stirred for 24 h at 90 °C in order to complete the re-ion exchange reaction between the unreacted Ag^+ ions and the Na^+ ions of the solution. After that, similar to previous stages, the suspended solids were filtered and washed with hot distilled water and also, repeatedly, with ethanol (5×20 ml). Next, the solids dried overnight at 100 °C in an oven. Solvent extraction was used to ensure complete removal of excess unreacted materials and any Ag^+ complexes adsorbed on the external surface of the zeolites. In this case, the solids were poured into an extraction thimble (Schleicher & Schuell, No. 603, 33 × 94 ml), laminated by a piece of cotton, and placed in a 250 ml soxhlet extractor. Ethanol was used as the solvent for 12 h of extraction. Finally, the found solid was dried for two days at 120 °C in a vacuum oven. Saddle brown powder consisting of $[Ag(diamine)]^+$ denoted as $[Ag(diamine)]^+$-NaY and, hereafter, named as Ag-2 was acquired after drying.

Part (3) Encapsulating macrocyclic ligands into the zeolite cavities through a template condensation reaction: 100 ml of methanol was poured in the reactor and 2 g of Ag-2 powder was added (at a ratio of 2 % (w/v)) and was stirred rigorously for 1 h at 700 rpm until a saddle brown suspension was obtained. Then, 100 mM of a diketone (or dione), acetylacetone (or 2,4-pentanedione) which is a colorless liquid, was added dropwise into the suspension and dissolved at 90 °C until its color changed firstly to brown and, after 24 h, through the completion of condensation reaction of diamine with diketone, became a dark brown suspension. Thereafter, the filtration, extraction, and drying procedures were done in a manner described above. Finally, a very dark brown complex powder consisting of encapsulated macrocyclic ligands denoted as $[Ag(hexa\text{-}aza)]^+$-NaY and, hereafter, easily named as Ag-3, was acquired after drying. Scheme 1 schematically represents the synthesis route described for encapsulating the polyaza macrocyclic ligands within the nano-reactors of zeolite Y by the template condensation of the diamine and diketone.

2.2.2. Membrane synthesis

The neat CA and, also, MMMs containing each of the particles (Ag-1, Ag-2, and Ag-3) were synthesized by a solution casting/solvent evaporation method. A rather volatile solvent, THF, was selected to conduct a uniform membrane formation through a reasonably fast evaporation/coagulation and simultaneously prevent particle sedimentation. Prior to membrane synthesis, the CA powder was dried at 80 °C for a day in an oven to remove adsorbed impurities. First, a predetermined value of filler was added to THF in a glass bottle with a plastic cap and continuously stirred for 24 h to ensure that all the particle agglomerates are broken apart and a homogeneous suspension is achieved. Next, priming was done by adding ~10 % of the total CA to the filler/THF suspension and stirring 4 h until a thin layer of CA covers each the solid filler. After filtration, the remaining ~90 % of

the CA was added gently while continuing the stirring up to 6 h. The priming or multi-stage addition of CA makes it possible to have the organic-organic compatibilizing effect of the previously formed CA layer. After that, the solution remained at room temperature about 30 min to attain a bubble-free solution. It was finally cast on a flat and clean glass plate by means of a casting knife with a gap of 300 μm. The flat-sheet film was dried 24 h at room temperature, which was followed by 48 h of drying in an vacuum oven with a temperature of 150 °C. The membranes with the thickness of about 30 μm were formed (measured by a digital micrometer (Mitutoyo®, Seisakusho, Tokyo, Japan) with an accuracy rate of ±1 μm).

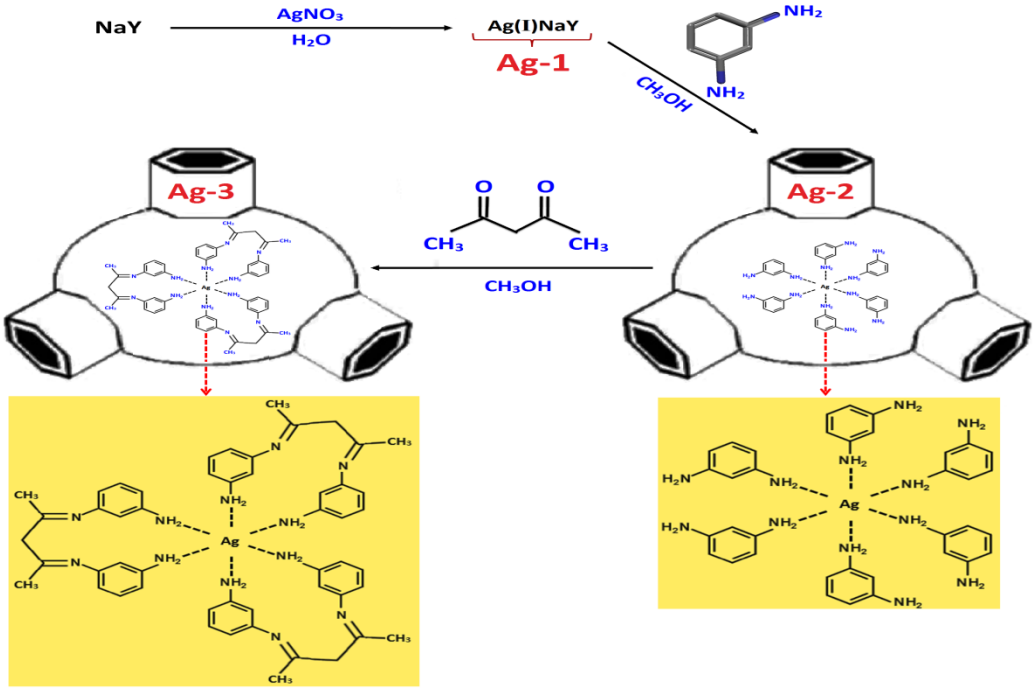

Scheme 1. Schematic representation of the SIB synthesis.

2.3. Gas permeation tests

The pure gas permeability in a Barrer unit (1 Barrer = 10^{-10} cm^3 (STP) cm/(cm^2 cmHg s)) at ~25 °C and 2–10 bar was calculated by a time lag method through the following equation [44-46]:

$$P = \frac{273.15 \times 10^{10} Vl}{AT(p_0 \times 76)}\left(\frac{dp}{dt}\right) \qquad (1)$$

where P is the permeability, V is the dead-volume of the downstream part of the homemade membrane holder (cm^3), l is the membrane thickness (cm), A is the effective membrane area (cm^2), T is the experimental temperature (K), p_0 is the feed pressure (atm), and dp/dt is the steady rate of pressure rise on the downstream side (atm/s).

The ideal selectivity of a membrane, α_{AB}, was calculated by dividing the permeabilities of the two pure gas components A and B measured in the same conditions [47]:

$$\alpha_{AB} = \frac{P_A}{P_B} \qquad (2)$$

2.4. Characterizations

Morphological observations of the membranes and filler particles were carried out by scanning electron microscopy (SEM). In the case of flat-sheet membranes, prior to analysis, they fractured in liquid nitrogen and sputter-coated with gold by a BAL-TEC SCD 005 sputter coater (BAL-TEC AG, Balzers,

Liechtenstein). SEM analyses of all the samples were performed with a KYKY-EM3200 (KYKY Technology Development Ltd., Beijing, China).

All the filler samples were studied by ultraviolet-visible diffuse reflectance spectroscopy (UV-vis DRS) with an Avantes AvaSpec-2048-TEC spectrometer (Avantes Inc., Apeldoorn, The Netherlands) in the wavelength range of 200 to 900 nm. Pure barium sulfate, $BaSO_4$, was used as a standard reference material.

The porous structure of filler particles was determined by N_2 low-temperature (76 K, liquid nitrogen) adsorption–desorption isotherms using TriStar II 3020 V1.03 analyzer (Micromeritics Instrument Co., Norcross, GA, USA). Specific surface area and volume of micro pores of the particles were calculated by the t-plot method. An average (cylindrical) pore diameter of $d_p=4V_p/S_{BET}$ was calculated by the desorption data. In this case, S_{BET} and V_p are the specific surface area and volume of micro pores, respectively, which were calculated by the standard Brunauer–Emmet–Teller (BET) method. Total desorption pore volume, V_p, was estimated at p/p_0 = 0.98, where p and p_0 represent the equilibrium and saturation pressures of nitrogen, respectively.

The X-ray diffraction (XRD) patterns of the samples were recorded on a X'Pert MPD wide-angle X-ray diffractometer (Philips, Eindhoven, Netherlands) at room temperature using α-rays emitted by cobalt (wave-length of 1.79 Å, accelerating voltage of 40 kV, and tube current of 40 mA, the scan range− the angle (2θ) of diffraction− of 3 to 70° with a step increment of 0.02° s^{-1}).

Fourier transform infrared-attenuated total reflectance (FTIR-ATR) of the membranes was recorded on a Perkin-Elmer Spectrum, Frontier model, Version 10.03.06 (Perkin-Elmer Instruments, Norwalk, CT, USA) in the range of 600-4000 cm^{-1}.

3. Results and discussion

3.1. Structure and morphology of particles

SEM. SEM images of NaY, Ag-1, Ag-2, and Ag-3 particles are depicted in Figure 1. NaY zeolite particles are composed of polygonal layered-like crystals formed with sharp edges. NaY particle sizes are around 1 μm with some agglomerates whose sizes rarely exceed 4-5 μm and are consistent with the average particle diameter of 1.22 μm and maximum particle size of 4.81 μm from the particle size analysis reported in the previous studies [37, 38, 48].

Ag-1 samples were also polygonal in shape; however, some of the crystals exhibited beveled edges. Higher alkalinity of the solution during the ion exchange reaction and lower dilution led to the preparation of cubic crystals with beveled edges [49]. In addition to Ag-1, Ag-2 and Ag-3 samples have some agglomerates such that the number and sizes increased from Ag-1 to Ag-3. This can result from the changes in electrical charge balance of the zeolites and the inducted electrostatic forces through the formation of Ag-ligands at Ag-2 and Ag-3 cavities.

Adsorption–desorption characteristics. Adsorption-desorption characteristics of the neat and complex particles are presented in Table 1. The micro-pore volumes and surface areas decreased remarkably, especially from Ag-1 to Ag-2, along with the trajectory illustrated for the SIB reaction steps in Scheme 1. Zeolite framework contains AlO_5^{-4} and SiO_4^{4-} tetrahedral linked to each other by the sharing of oxygen atoms in each corner and one Al or Si atom at the center of the tetrahedron. Na^+ or other mono- or di-positive ions are located mainly at the Al-rich center of zeolite crystals to maintain the

electroneutrality of the zeolite by stabilizing ≡Si–O–Al^{-}≡ bonds [10, 50]. It has been frequently stated that ion exchange reaction of a faujasite-type zeolite coincides with a decrease in Al content in the zeolite structure and an increase in Si/Al ratio [51-54]. Dealumination decreases the unit cell size and, consequently, surface area and pore volume of the zeolite. In the case of Ag-2 and Ag-3, a decrease in surface area and pore volume was quite predictable due to the occupation of (some) zeolite pores by Ag-ligand complexes.

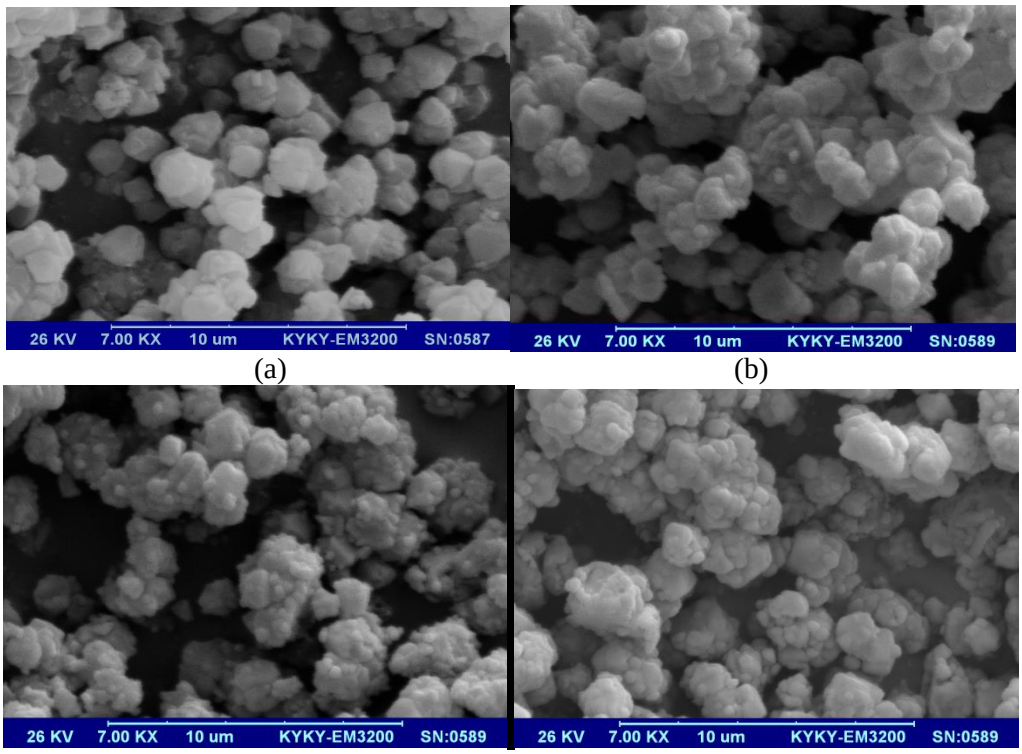

Figure 1. SEM images of the (a) NaY [36], (b) Ag-1, (c) Ag-2, and (d) Ag-3 particles.

Table 1
Adsorption-desorption characteristics of the particles.

Sample	NaY	Ag-1	Ag-2	Ag-3
Micro-pore volume (cm^3/g)	0.285	0.240	0.089	0.067
Micro-pore surface area (m^2/g)	596	534	205	135
Average pore diameter (Å)	19.2	19.6	20.5	20.4

Table 1 shows also a small increase in the average micro-pore diameter. In spite of the higher ionic radius of Ag^+ (1.15 Å) in comparison with Na^+ (1.02 Å) which induces a lower particle pore size, a distortion of tetrahedral sites of the pure NaY zeolite during the ion exchange and coordination reactions can be a reason for a small increase (~1 Å) in the pore diameters [55].

DRS. Figure 2 shows the diffuse reflectance spectra of all the particles. NaY zeolite shows a broad absorption band with a minimum at 261 nm in the UV region. It refers to Na–O bonds in the zeolite framework that can absorb the UV light. By loading the silver ions, intensity and minimum wavelength of the 261 nm band shift to lower values and also a new absorption band observes at 460 to 563 nm. The appearance of a couple of bands can result from occupying the zeolite framework by the

Ag^+ ions at different sites [56]. The former is assigned to a charge transfer transition between $4d^{10}$ and $4d^95s^1$ levels of Ag^+, and the latter is attributed to a partial reduction of Ag^+ ions and aggregation of the metal clusters [57-60]. The formation of $Ag_n^{\delta+}$ (n=2-8) clusters with different sizes in faujasite-type zeolites has been reported in the case of the degree of ion exchange and the reduction conditions [59, 61-64]. In the case of Ag-2 and Ag-3 samples, no distinctive absorptions can be observed due to overlapping of the ligand field and the charge transfer absorptions. However, of note, the lowest absorption bands of the spectra for Ag^+ complexes are assigned to $d\rightarrow\pi^*$ charge transfer in accordance with other studies on α-diimine complexes [65, 66]. In the visible region for Ag-2 and Ag-3 samples, the ligand field transitions severely lowered Ag^+ absorption intensity and wavelength and, further, made changes in the slope of curves as compared to Ag-1. For Ag-2, a broad, narrow absorption band can be seen in the region of 470 to 590 nm with a maximum at 528 nm, which can be attributed to hexahedrally coordinated Ag^+ ligands.

The properties of most probable products in the SIB synthesis in the present study were calculated by molecular mechanics method using Spartan software (Wavefunction Inc., Irvine, CA, USA), and the results are summarized in Table 2 and Scheme 2. According to the position of silver as a transient metal in the elemental periodic table, the stable molecular structures for the synthesized Ag-ligand complexes include two coordination numbers of 4 and 6 (Scheme 2).

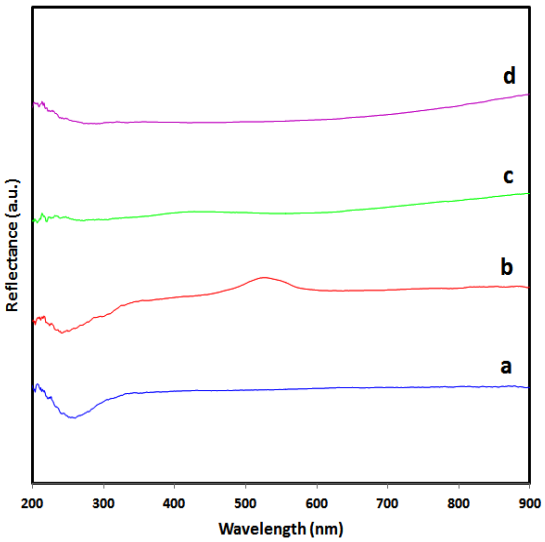

Figure 2. DRS spectra of the (a) NaY, (b) Ag-1, (c) Ag-2, and (d) Ag-3 particles.

The minimum energy (used for optimization of the geometry) for coordination number of 6 is -1124 kJ/mol, much lower than -89 kJ/mol for the other. Therefore, the coordination number of 6 for the Ag-ligand complexes is confirmed by molecular modeling. It is worth noting that despite its large dimensions (~14×17 Å), the complex can be encapsulated properly in the cavities of the zeolite Y (~20 Å, from the BET results) through the SIB synthesis, although encapsulation of larger complexes (with a size of 19 Å) through their distortions in the NaY supercages (~13 Å in diameter) due to the intrazeolitic constraint inside the cages was reported in other works [67]. A schematic representation of the encapsulated complex in a supercage of the zeolite Y is illustrated in Scheme 2. Along with better properties of 6-coordinated complex as compared to the 4-coordinated one, a distinct difference can be observed in dipole moments, 4.98 vs. 3.83 Debye (Table 2). The larger dipole moment is an important factor for a better intermolecular interaction between CO_2 and complex molecule.

Table 2
Properties of the probable Ag-ligand complexes formed into the zeolite Y cavities through the SIB synthesis.

Sample	Formula	Molecular weight (amu) [1]	Area ($Å^2$) [2]	Volume ($Å^3$) [2]	Polar surface area ($Å^2$) [2]	Ovality [2]	Molecular mechanical energy (kJ/mol) [2]	dipole moment (Debye) [2]
Ag complex with the coordination number of 4	$C_{34}H_{36}AgN_8$	664	635	613	92	1.82	-89	3.83
Ag complex with the coordination number of 6	$C_{51}H_{54}AgN_{12}$	943	900	911	113	1.98	-1124	4.98

[1] atomic mass unit

[2] through generations of the 3D CPK models (ball-and-spoke) of the complexes; CPK is a space-filling model that considers each molecule composed of some spheres with the radii as Van der Waals distances of two adjacent atoms. Molecular area, volume, polar surface area (PSA), polarizability, ovality, dipole moment, and structural energies can be calculated by the CPK model. Polar surface area is the area of oxygens, nitrogens, and all the hydrogens linked to these atoms. Ovality index represents the deviation of a molecule from the spherical shape, since the spherical shape has the minimum surface with the ovality as unity.

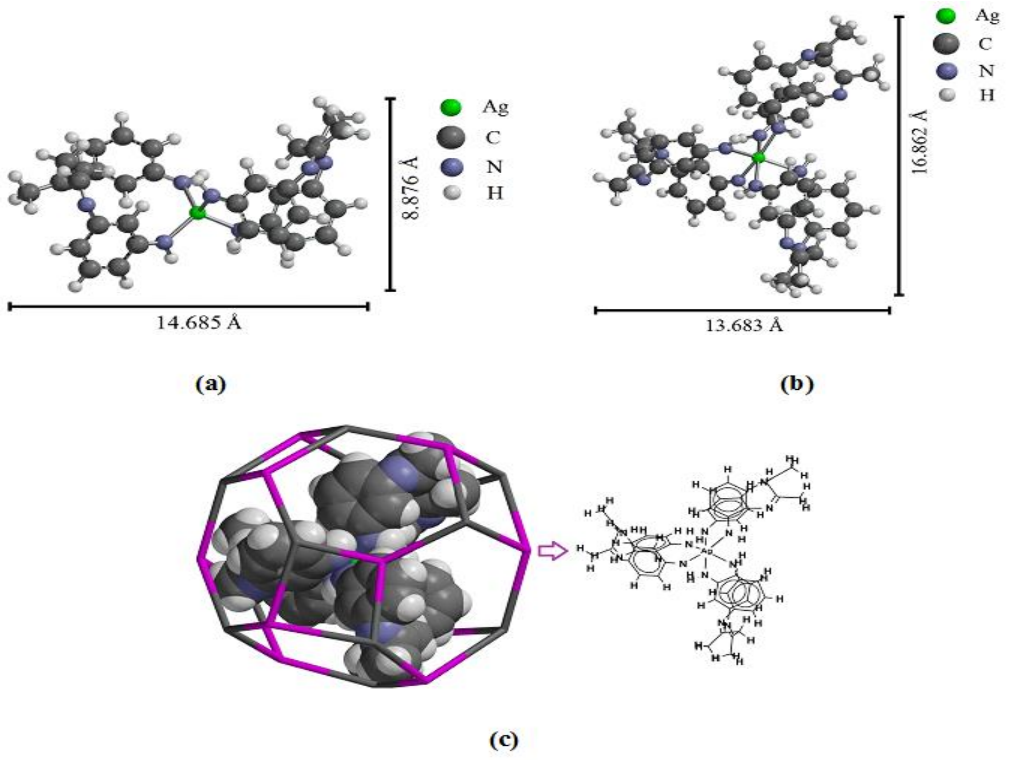

Scheme 2. The molecular structures of complexes.

XRD. Figure 3 shows the XRD spectra of all the particles, NaY, Ag-1, Ag-2, and Ag-3. In the case of NaY zeolite, all of the corresponding characteristic peaks assigned to the 3D crystalline structure of an FAU zeolite Y were depicted. The peaks occurred respectively at 2θ positions of 7.2, 11.8, 13.8, 18.2, 21.7, 23.7, 27.6, 31.6, 34.6, 35.9, 36.7, 37.9, and 39.8°, according to the standard card JCPDS No. 43-0168. It has been repeatedly occurred in other works [48, 68-70], revealing the purity of the NaY zeolite. All the peaks were also repeated for Ag-1 with only low differences in the peak intensities, where they were lowered due to the decrease of crystallinity of zeolite during the ion exchange reaction. Indeed, dealumination through the ion exchange treatment coincided with a small

lattice collapse in the zeolite [71]. It is in good agreement with the SEM and BET results. In the case of Ag-2 and Ag-3, a decrease in the peak intensities as compared to NaY was also observed, showing a decrease in crystallinity. Three peak intensities related to 2θ=11.8, 13.8, and 18.2° in NaY zeolite are illustrated by I1, I2, and I3, respectively, which are representatives for the cations located in NaY. They are arranged for the NaY in the order of I3>>I1>I2, such that for the Ag-1, Ag-2, and Ag-3, it changes to I3>>I2>I1. It arises from the rearrangements of the zeolite structure due to the substitution of the large numbers of Na+ with the Ag+ cations and also the encapsulation of the large Ag-ligand complexes in the cavities [72]. A similar discussion can be also proposed for the peaks located at 2θ=36.7, 37.9, and 39.8°. In addition, for Ag-2 and Ag-3 particles, two sharp peaks at 2θ= 44.5 and 51.9° can be observed that refer to crystalline plates in the silver cubic crystals. They can be attributed to the metallic Ag+ clusters, which are reduced to Ag0 on the zeolite surfaces [72-74], which are in agreement with the DRS results. It was demonstrated that proper interaction of amino groups and the metal surface resulted in the formation of the stable complexes [75].

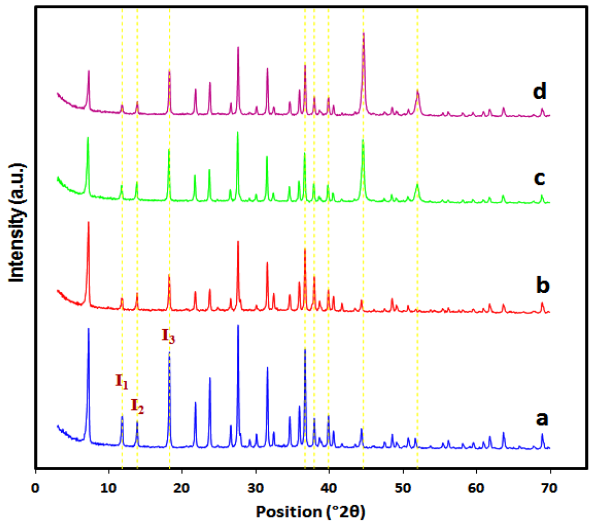

Figure 3. XRD spectra of (a) NaY, (b) Ag-1, (c) Ag-2, and (d) Ag-3 particles.

3.2. Characterization of MMMs

SEM. SEM images of the fractured cross-sections of pure CA and the MMMs containing 15 wt % of Ag-1, Ag-2, and Ag-3 are depicted in Figure 4a-d. It is worth mentioning that the value of 15 wt % filler loading was selected because each series of the prepared MMMs showed its best gas separation performance at this point. As can be observed, a uniform, defect-free and dense structure was formed for pure CA (Figure 4a). Some small crazes were observed for cross-sectional images of particles-loaded MMMs. Indeed, the numbers and sizes of the crazes are reduced from Ag-1 to Ag-3 loaded MMMs (Figure 4b-d). It can be due to a better electric charge distribution of Ag-3 particles, and, hence, better compatibility with the membrane matrix that results in decreasing the tension during solvent evaporation in CA/Ag-3 MMM's formation. Moreover, an appropriately good dispersion of the particles is indicated for the MMMs, especially for that of contained Ag-3 particles. It may be due to a better electrostatic interaction between Ag-3 and CA matrix as compared to the other particles. A few agglomerates of particles with 4-5 μm in size were also formed in the MMMs, where the number and sizes are not large enough to make a serious problem in gas transport. Nonetheless, it makes considerable problems in higher loadings as will be reflected in gas transport data of the following sections.

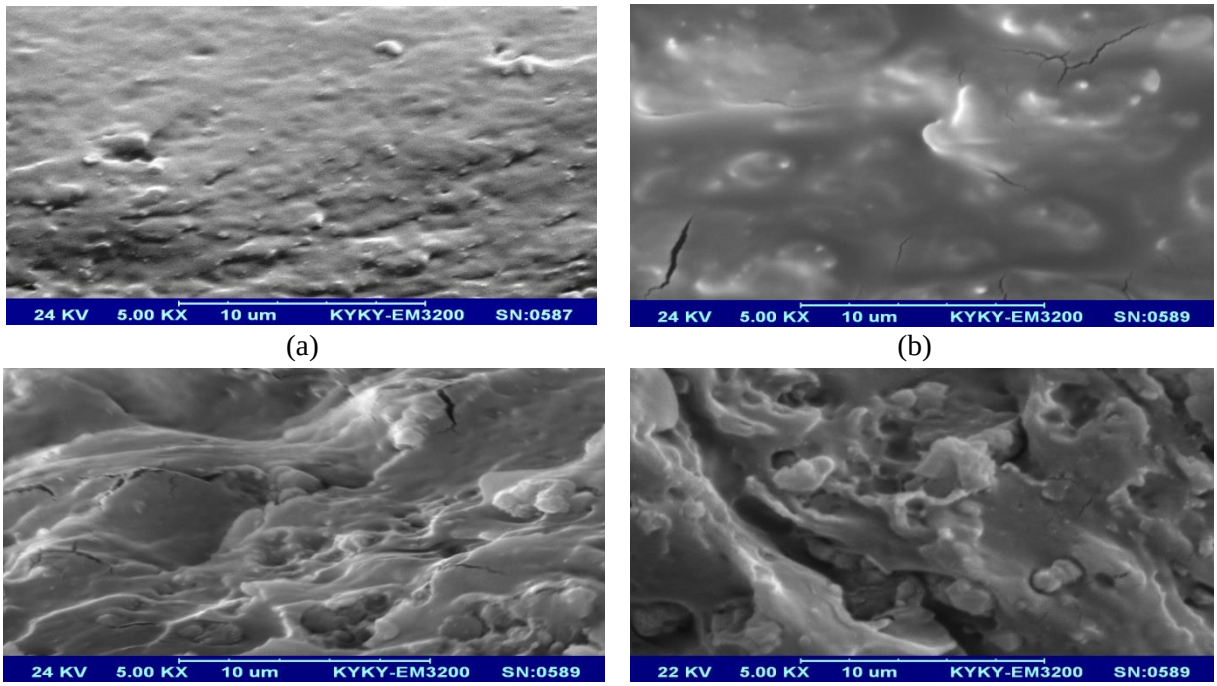

(a) (b)

(c) (d)

Figure 4. SEM images of the (a) CA, (b) CA/Ag-1, (c) CA/Ag-2, and (d) CA/Ag-3 membranes.

FTIR. FTIR-ATR spectra of pure CA and the MMMs containing 15 wt % of Ag-1, Ag-2, and Ag-3 are shown in Figure 5a-d. Figure 5a shows a broad absorption band at around 3484 cm^{-1} for pure CA related to OH^- stretching vibrations of the hydroxyl groups. It almost disappears in Figure 5b-d for all the MMMs' spectra due to the hydrogen bonding reaction between silanol groups (SiOH) of the external particle surfaces with the OH^- of CA. Generally, by inserting all the particles into the CA matrix, all the band intensities decrease. It appears that a decrease is lowered from Ag-1 loaded MMM (Figure 5b) to Ag-3 loaded one (Figure 5d). However, Si–O and Al–O stretching vibrations of the zeolite structure of the hybrid particles occurred respectively in the ranges of 1100-1000 cm^{-1} and 800-600 cm^{-1} and led to a lower decrease in the corresponding intensities of C–O stretching vibrations of CA. Otherwise, all the characteristic bands of CA are shown in accordance with the literature [36, 37, 39].

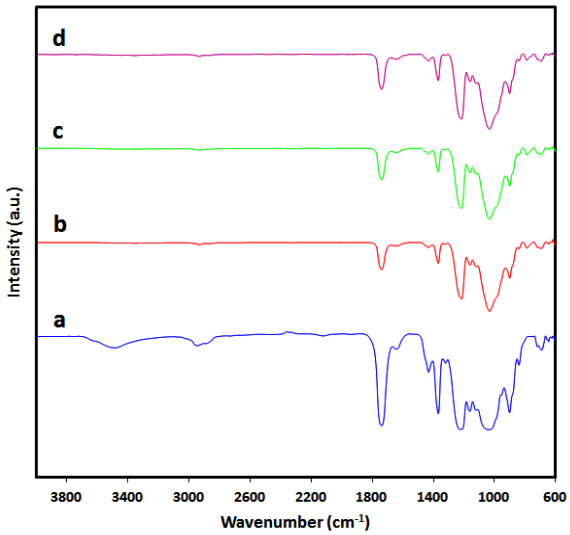

Figure 5. FTIR-ATR spectra of (a) CA, (b) CA/Ag-1, (c) CA/Ag-2, and (d) CA/Ag-3 membranes.

XRD. XRD spectra of pure CA and the MMMs containing 15 wt % of Ag-1, Ag-2, and Ag-3 are illustrated in Figure 6a-d. Two broad crystalline peaks at 2θ=10 and 22° are distinguished for pure CA in Figure 6a. Inserting the zeolite hybrid particles into the CA matrix leads to a slight decrease in the intensities of the two characteristic peaks of CA, which means lower crystallinity of the

MMMs in comparison with the CA membrane (Figure 6b-d). Moreover, all the characteristic peaks of the hybrid particles (see Figure 3) are also shown in Figure 6b-d for the corresponding MMMs. The d-spacing of 7.37 and 4.04 Å corresponding to 2θ=10 and 22° for pure CA is changed to 7.41 and 4.73 Å for CA/Ag-1, 7.44, and 4.76 for CA/Ag-2 and 8.78 and 4.76 for CA/Ag-3 MMMs. The increase of d-spacing of zeolite hybrid loaded MMMs shows an increase in interchain spacing of the MMMs compared to the pure CA and, in turn, a higher fractional free volume and a better molecular transport across the MMMs. In fact, the lower crystalline nature or higher amorphous structure of the MMMs coincides with a decrease in the polymer chain packaging and will result in higher gas permeability.

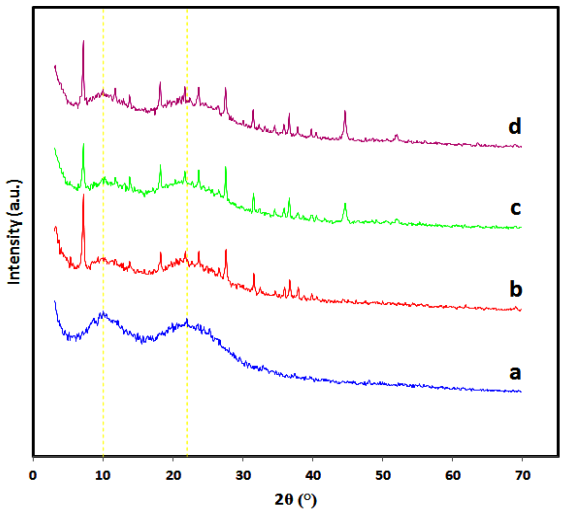

Figure 6. XRD spectra of (a) CA, (b) CA/Ag-1, (c) CA/Ag-2, and (d) CA/Ag-3 membranes.

3.3. Tests of gas permeability of the MMMs

Figure 7 shows the permeability/selectivity behavior of the nano-porous hybrid filler incorporated MMMs (0-20 wt % Ag-3 loadings) in the pressure range of 2-10 bar. As can be seen in Figure 7a, an increase in filler content and a decrease in pressure lead to the increase of CO2 permeability. This increase is firstly steeper and gradually develops with a mild slope. The N_2 permeability also increases with an increase in filler content; however, it shows somewhat an opposite behavior with respect to the pressure increase. In addition, with an increase in filler loading, N_2 permeability increases firstly with a mild slope up to 10 wt % and, then, slightly decreases in 15 wt %; next, it experiences a remarkable growth at 20 wt % (Figure 7b). Various observations originate from some different phenomena that are explained as follows:

CO_2 and N_2 are non-polar molecules with a slight difference in kinetic diameters, which can be separated reasonably based on the size exclusion. CO_2 is a linear, symmetric, three-atomic molecule (O=C=O) and does not have a permanent dipole moment; however, it has two transition dipole moments (a couple of C=O bonds) that form a substantial quadrupole moment (two couples of C–O bonds) operating over a much shorter distance than dipole interactions [76-78]. This induces considerable differences in the electronic properties of CO_2 compared to N_2. Higher polarizability (1.49:1) [79] and, especially, the higher quadrupole moment (2.85:1) [80] of CO_2 compared to N_2 enable the design of CO_2–philic sorbents with a strong affinity for CO_2 through the dipole-quadrupole interactions [81]. Therefore, CO_2 with an electron–deficient carbon atom as a Lewis acid could have favorable interactions with the electronegative metal-organic complexes as Lewis bases, leading to strong acid-base interactions, while N_2 is not affected [82].

Gas solubility in polymeric membranes depends on the gas condensability, gas/polymeric matrix interactions, and also somehow on the fractional free volume (FFV) of the polymer. However, gas diffusivity depends on the gas molecular size, segmental

mobility of polymer chains, and strongly on the FFV in the polymer [21, 83-86]. In the case of CO_2 in a glassy cellulose acetate matrix, the most probable interaction comprises a Lewis acid-base nature, where the carbon atom of the CO_2 molecule acts as an electron acceptor and the carbonyl oxygen atom in the polymer as an electron donor. Roughly speaking, an increase in the membrane polar groups–either by organic or inorganic additives–mostly results in decreasing the free volume or increasing the polymer chain rigidity, while it increases CO_2 solubility and decreases diffusivity. In addition, the affinity of the polar groups to CO_2 molecule can restrict the pathways for further CO_2 diffusion, especially at higher CO_2 pressures.

Herein, a *facilitated transport mechanism* in addition to the simple *solution-diffusion mechanism* involved the CO_2 gas transport across the MMMs. In the facilitated transport, CO_2 acts as an electron donor, while the SIB synthesized encapsulated molecules in zeolite cavities serve as an acceptor in a reversible complexation reaction; CO_2 reacts at one reactive site of an SIB synthesized encapsulated carrier to form "CO_2-SIB complex" and, then, hops to another reactive site of the carrier or the one for an adjacent carrier, where a decomplexation reaction along with a recomplexation occurs. Accordingly, CO_2 is well transported by a "hopping" mechanism, a *reactive diffusion* towards downstream of the membrane. This can effectively enhance sorption into and desorption from the zeolite particles and, hence, accelerate the species transport.

In porous zeolite Y particles with the pores somewhat larger than 1.5 nm, *surface-activated diffusion* can become another mechanism involved in species transport. In this phenomenon, the pore walls strongly adsorb some of the molecules that can move from a sorption site to an adjacent sorption site. The adsorbed molecule encompasses additional kinetic energy at a given distance from the surface that surpasses the energy barrier of a given elevation on the surface (activated diffusion jumps) [87]. The interacting CO_2 molecules as compared to the non-interacting N_2 molecules can be transported through the zeolite particles via the *surface-activated diffusion* simultaneously with the *Fickian diffusion* both for CO_2 and N_2 molecules.

In the case of CO_2/N_2 selectivity (Figure 7c), an increasing behavior up to 15 wt % of the filler loading is observed, which is followed by a considerable decrease at 20 wt %. As can be seen, the best separation performance of the MMMs obtained for the MMM contained 15 wt % Ag-3 with a selectivity increase of 40.28 % as compared to the pure CA membrane at 2 bar. This corresponds to the CO_2 permeability increase of 45.71 %. A combination of the following factors describes the selectivity data in Figure 7c:

The extra-framework cations (here, Na^+ and Ag^+) used for electroneutralizing the zeolite crystals can influence surface sorption ability. Different cations with a variety in the polarizability produce zeolites varying in their effective pore diameters and volumes. They also affect the local electrical fields and basicity of the zeolites. The addition of organic groups, such as alkyls, alkyl amines, etc., increases the cation radii and, hence, decreases their polarizability that results in weaker interactions with CO_2 molecules. Moreover, the porous areas and volumes in the presence of organic linkages decrease, which can lead to lower surface sorption of CO_2 [88]. On the other hand, the basicity of alkyl amines

encapsulated in the zeolite is one or two orders of magnitudes higher than that of the pure zeolite. This is in conformity with the fact that N-containing (N: nitrogen) hybrid zeolites are frequently suggested as a basic adsorbent/catalyst. Furthermore, the aromatic-containing encapsulated zeolites (like Ag-2 particles) are more fascinating because of their ability to produce a wide variety of chemically active sites, e.g., with the completion of SIB synthesis (Ag-3 particles) [89]. The basic active site has a proper interaction with CO_2 molecule as a Lewis acid. In addition, the pore entrances of zeolite Y (~0.74 nm) are large enough as compared to CO_2 and N_2 kinetic diameters (0.33 and 0.36 nm, respectively) for passing through the activated diffusion mechanism [90-92]. CO_2 with a smaller size can possess better transport in the case. Therefore, it can be expected that more particle loadings support more CO_2 transport from both the acid-base interaction and activated diffusion mechanisms that enhance the CO_2/N_2 selectivity. At higher particle loadings, some agglomerates appear in the MMM matrix whose numbers and sizes would be more considerable at 20 wt % [37]. It is a limit in particle dispersion where they coalesce into each other and form some agglomerates that increasingly result in the formation of non-selective transport pathways across the membrane matrix. This is known as *percolation threshold* for the proper particle dispersion that affects considerably molecular transport of penetrant species across the MMMs. Beyond the percolation limit, a convective flow of molecules throughout the MMM without adequate selectivity will occur.

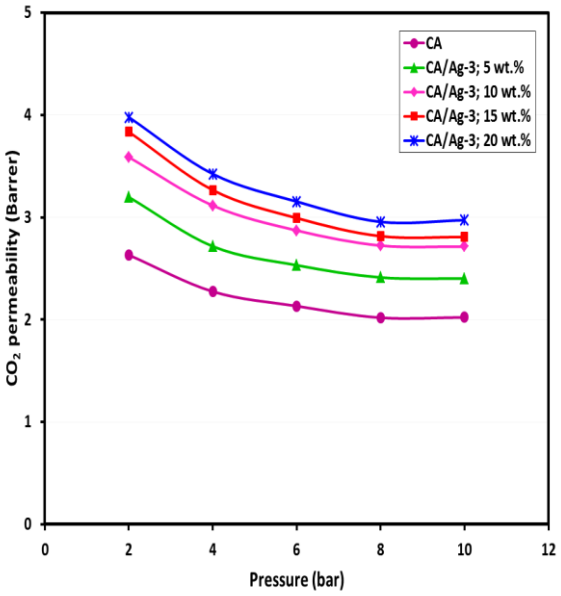

(a)

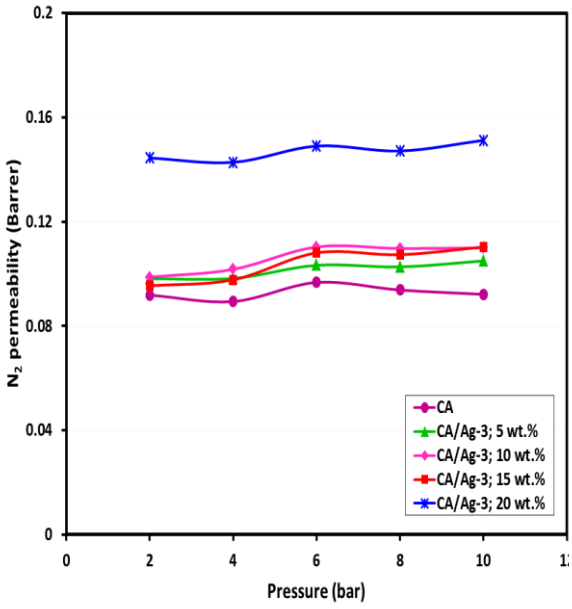

(b)

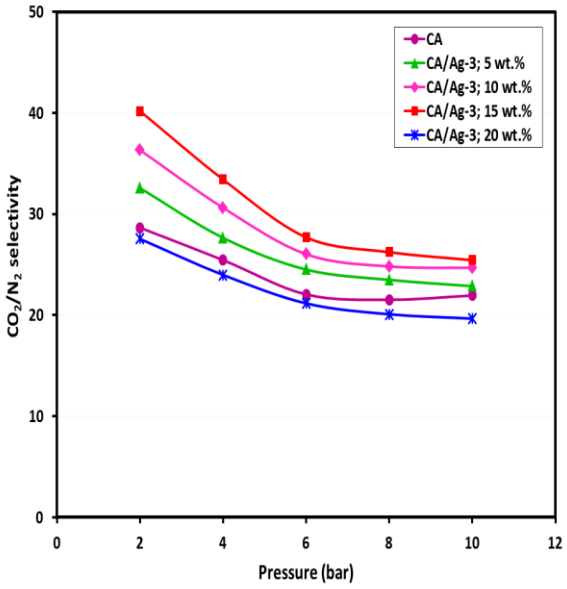

(c)

Figure 7. (a) The CO_2 permeability, (b) the N_2 permeability, and (c) the corresponding CO_2/N_2 selectivity at different Ag-3 loadings in terms of pressure.

The effect of pressure on selectivity can be explained as follows. It has been demonstrated that the N_2 adsorption, compared to other gases, in hybrid zeolites is lower than that in pure zeolites [89]. Therefore, CO_2/N_2 solubility selectivity of hybrid zeolites is more than unity. Since diffusivity is more dependent on temperature rather than on the pressure, no considerable changes in gas diffusivity of the hybrids with the pressure increment from 2-10 bar at a constant temperature can be expected. Plasticization (and its effect on chain packing and free volume) of CA matrix becomes significant as CO_2 pressure increases. CO_2-induced plasticization decreases CO_2/N_2 selectivity as the pressure increases in the range of 2-10 bar, just below the plasticization pressure (=12.76 bar obtained in the previous work for the annealed CA membrane [39]). For glassy polymers and the related MMMs, it is frequently expressed that an increase in the CO_2 pressure in this region exerts pressure on the polymer chains and increases its chain packing density and, in turn, decreases CO_2 permeability and CO_2/N_2 selectivity [93]. The plasticization-induced reduction in CO_2/N_2 selectivity can be compensated to some extent by the matrix rigidifying at higher particle loadings (Figure 7c).

3.4. Comparison of the MMM performances

Figure 8 shows a comparison between the gas separation performances of the 15 wt % Ag-1, Ag-2, and Ag-3 embedded MMMs and the neat CA membrane in the pressure range of 2-10 bar and 25 °C. As can be observed, all the MMMs have better CO_2 permeability and CO_2/N_2 selectivity than the neat CA polymer. Generally, at 2 bar and 25 °C, the MMM with 15 wt % Ag-3 shows the best gas separation performance among the others. It respectively provides CO_2 permeability and CO_2/N_2 selectivity of 45.71 % and 40.28 % higher than the pure CA membrane. Although the permeability and selectivity of CA/Ag-2 and CA/Ag-3 MMMs are roughly closer together at higher pressures, the good chemical stability of Ag-3 hybrid complexes, as well as the proper reversible complexation/decomplexation reaction of CO_2-Ag-3 in comparison with the CO_2-Ag-2, makes Ag-3 a promising filler for embedding in the future MMMs; particularly, it can be proposed as a good candidate for economically implemented MMMs in post-combustion CO_2 capture, a process that deals with a low partial pressure of CO_2 at flue gas streams.

3.5. Comparison with other works

Table 3 presents the results of a comparison between the performances of the prepared membranes in this work and the other CA-based MMMs in the literature. As can be seen, the CA/Ag-3 MMM reveals higher selectivity among the various MMMs. In most cases, an

increase in filler loading enchances permeability, while selectivity experiences considerable loss. However, the CA-based MMMs in this work exhibit improvements both in the permeability and selectivity, while the others experience considerable selectivity loss. By incorporating Ag-3 particles where a polyaza macrocyclic Ag-ligand complex was encapsulated into the zeolite Y, the selectivity was considerably enhanced. Certainly, the most important advantage of the Ag-3 loaded MMMs is that they take the gentle properties of novel SIB-synthesized metal-organic filler for membrane gas separation.

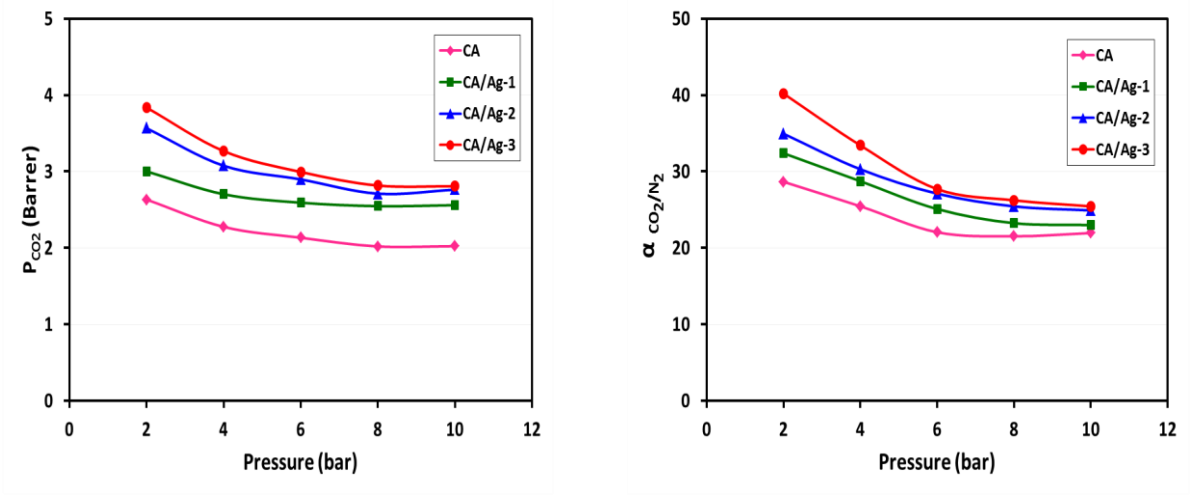

(a) (b)

Figure 8. A comparison between the gas separation performances of the MMMs and the neat CA membrane in the pressure range of 2-10 bar and at 25 °C.

Table 3
A comparison between the performances of the selected CA-based MMMs.

Membrane	Filler loading (wt %)	T (°C)	p (bar)	P_{CO2} (Barrer)	$\alpha_{CO2/N2}$	Ref.
CA/NH_2-MIL-53(Al)	15	25	3	6.7 (GPU)	12.00	[94]
CA/NH_2-MIL-53(Al)	15	25	3	52.6	23.4	[95]
CA/SAMH-3	4	25	4.5	10.36	--	[96]
CA/MWCNTs-P	0.1	25	2	146.70 (GPU)	5.56	[97]
CA/MWCNTs-F	0.1	25	2	741.67 (GPU)	40.18	[97]
CA/Co(II)–NaY	15	25	4	3.28	29.2	[37]
CA/NaY-sm	20	25	2	4.63	28.07	[36]
CA/NaY	20	25	4	4.87	25.00	[39]
CA	0	25	2	2.63	28.65	This work
CA/Ag-3	15	25	2	3.84	40.20	This work

4. Conclusions

This study successfully showed that the encapsulated polyaza macrocyclic Ag-ligand complexes in zeolite Y cavities, which are synthesized through the ship-in-a-bottle (SIB) method, can be beneficial as new nano-porous hybrid fillers for embedding in the glassy cellulose acetate (CA) membrane matrix in order to prepare advanced mixed matrix membranes (MMMs) for CO_2 separation. The fabricated MMMs exhibit suitable enhancements simultaneously in the permeability (45.71 %) and selectivity (40.28 %) of the pristine polymeric membrane.

Therefore, the technique will be of interest for future membrane engineering towards industrial applications.

Acknowledgments

The financial supports of Arak University, Amirkabir University of Technology, and Tarbiat Modares University are gratefully acknowledged. Valuable assistances in preparation of the filler samples by Mr. Mohammad Rokhsaran are also acknowledged. The expert assistance of Mr. Mahmood Andache with the BET measurements is also sincerely appreciated.

Nomenclature

Abbreviations

AAS	atomic absorption spectrophotometer.
BET	Brunauer–Emmet–Teller.
CA	cellulose acetate.
DRS	diffuse reflectance spectroscopy.
FTIR-ATR	Fourier transform infrared-attenuated total reflectance.
MMM	mixed matrix membrane.
MOF	metal organic framework.
$NaNO_3$	sodium nitrate.
NaY	sodium Y zeolite.
SEM	scanning electron microscopy.
SIB	ship-in-a-bottle.
THF	Tetrahydrofuran.
XRD	X-ray diffraction.

References

[1] Forster, P. M. and Cheetham, A. K., "Hybrid inorganic-organic solids: An emerging class of nanoporous catalysts", *Top. Catal.*, **24**, 79 (2003).

[2] Ebadi Amooghin, A., Mashhadikhan, S., Sanaeepur, H. R., Moghadassi, A., Matsuura, T. and Ramakrishna, S., "Substantial breakthroughs on function-led design of advanced materials used in mixed matrix membranes (MMMs): A new horizon for efficient CO_2 separation", *Prog. Mater. Sci.*, **102**, 222 (2019).

[3] Sanaeepur, H. R., Ahmadi, R., Ebadi Amooghin, A. and Ghanbari, D., "A novel ternary mixed matrix membrane containing glycerol-modified poly(ether-block-amide) (Pebax 1657)/copper nanoparticles for CO_2 separation", *J. Membr. Sci.*, **573**, 234 (2019).

[4] Herron, N., Stucky, G. D. and Tolman, C. A., "The reactivity of tetracarbonylnickel encapsulated in zeolite X: A case history of intrazeolite coordination chemistry", *Inorg. Chim. Acta*, **100**, 135 (1985).

[5] Kahlen, W., Wagner, H. H. and Holderich, W. F., "Zeolite effect in the enantioselective transhydrogenation over a Co-salen "ship-in-the-bottle" complex", *Catal. Lett.*, **54**, 85 (1998).

[6] Herron, N., "A cobalt oxygen carrier in zeolite Y: A molecular "ship in a bottle"", *Inorg. Chem.*, **25**, 4714 (1986).

[7] Jia, Y., Shmakov, S. N., Register, P. and Pinkhassik, E., "Size-selective yolk-shell nanoreactors with nanometer-thin porous polymer shells", *Chem. Eur. J.*, **21**, 12709 (2015).

[8] Peng, J., Lan, G., Guo, M., Wei, X., Li, C. and Yang, Q., "Fabrication of efficient hydrogenation nanoreactors by modifying the freedom of ultrasmall platinum nanoparticles within yolk-shell nanospheres", *Chem. Eng. J.*, **21**, 10490 (2015).

[9] Wu, C. D. and Zhao, M., "Incorporation of molecular catalysts in metal-organic frameworks for highly efficient heterogeneous catalysis", *Adv. Mater.*, **29**, 1605446 (2017).

[10] Corma, A. and Garcia, H., "Supramolecular host-guest systems in zeolites prepared by ship-in-a-bottle

synthesis", *Eur. J. Inorg. Chem.*, **6**, 1143 (2004).

[11] Liu, J., Qiao, S.Z., Chen, J. S., Lou, X. W. D., Xing, X. and Lu, G. Q. M., "Yolk/shell nanoparticles: new platforms for nanoreactors, drug delivery and lithium-ion batteries", *Chem. Commun.*, **47**, 12578 (2011).

[12] Fujie, K. and Kitagawa, H., "Ionic liquid transported into metal-organic frameworks", *Coord. Chem. Rev.*, **307**, 382 (2016).

[13] Gkaniatsou, E., Sicard, C., Ricoux, R., Mahy, J. -P., Steunou, N. and Serre, C., "Metal-organic frameworks: A novel host platform for enzymatic catalysis and detection", *Mater. Horiz.*, **4**, 55 (2017).

[14] Matsuda, R. K., Kitagawa, R., Kubota, S., Belosludov, Y., Kobayashi, R. V., Sakamoto, T. C., Chiba, H., Takata, T., Kawazoe, M. and Mita, Y., "Highly controlled acetylene accommodation in a metal-organic microporous material", *Nature*, **436**, 238 (2005).

[15] Seki, K., "Design of an adsorbent with an ideal pore structure for methane adsorption using metal complexes", *Chem. Commun.*, 1496 (2001).

[16] Caro, J., "Are MOF membranes better in gas separation than those made of zeolites?", *Curr. Opin. Chem. Eng.*, **1**, 77 (2011).

[17] Zhang, Y., Musselman, I. H., Ferraris, J. P. and Balkus, K. J., "Gas permeability properties of Matrimid® membranes containing the metal-organic framework Cu–BPY–HFS", *J. Membr. Sci.*, **313**, 170 (2008).

[18] Zornoza, B., Tellez, C., Coronas, J., Gascon, J. and Kapteijn, F., "Metal organic framework based mixed matrix membranes: An increasingly important field of research with a large application potential", *Micropor. Mesopor. Mat.*, **166**, 67 (2012).

[19] Ebadi Amooghin, A., Sanaeepur, H. R., Zamani Pedram, M., Omidkhah, M. R. and Kargari, A., "New advances in polymeric membranes for CO_2 separation", Polymer science: Research advances, practical applications and educational aspects, Méndez-Vilas, A. and Solano-Martín, A. Eds., Formatex Research Center, Badajoz, Spain, p. 354 (2016).

[20] Adams, R., Carson, C., Ward, J., Tannenbaum, R. and Koros, W., "Metal organic framework mixed matrix membranes for gas separations", *Micropor. Mesopor. Mat.*, **131**, 13 (2010).

[21] Rezakazemi, M., Ebadi Amooghin, A., Montazer-Rahmati, M. M., Fauzi Ismail, A. and Matsuura, T., "State-of-the-art membrane based CO_2 separation using mixed matrix membranes (MMMs): An overview on current status and future directions", *Prog. Polym. Sci.*, **39**, 817 (2014).

[22] Ferrey, G. and Serre, C., "Large breathing effects in three-dimentional porous hybrid matter: Facts, analyses, rules and consequences", *Chem. Soc. Rev.*, **38**, 1380 (2009).

[23] Li, K., Olson, D. H., Seidel, J., Emge, T. J., Gong, H., Zeng, H. and Li, J., "Zeolitic imidazolate frameworks for kinetic separation of propane and propene", *J. Am. Chem. Soc.*, **131**, 10368 (2009).

[24] Li, S., Falconer, J. L. and Noble, R. D., "Improved SAPO-34 membranes for CO_2/CH_4 separations", *Adv. Mater.*, **18**, 2601 (2006).

[25] Koros, W. J. and Zhang, C., "Materials for next-generation molecularly selective

synthetic membranes", *Nat. Mater.*, **16**, 289 (2017).

[26] Huang, L., Wang, H., Chen, J., Wang, Z., Sun, J., Zhao, D. and Yan, Y., "Synthesis, morphology control, and properties of porous metal-organic coordination polymers", *Micropor. Mesopor. Mat.*, **58**, 105 (2003).

[27] Hess, S. C., Grass, R. N. and Stark, W. J., "MOF channels within porous polymer film: Flexible, self-supporting ZIF‑8 poly(ether sulfone) composite membrane", *Chem. Mater.*, **28**, 7638 (2016).

[28] Sanaeepur, H. R., "Tailoring "ship in a bottle" synthesized metal-organic nanoporous hybrid materials embedded in a mixed matrix membrane for CO_2 separation", Petrochemical Engineering Department, Amirkabir University of Technology (Tehran Polytechnic), Mahshahr Campus, Mahshahr, Iran, (2015).

[29] Hosseinkhani, O., Kargari, A. and Sanaeepur, H. R., "Facilitated transport of CO_2 through Co(II)-S-EPDM ionomer membrane", *J. Membr. Sci.*, **469**, 151 (2014).

[30] Ebadi Amooghin, A., Omidkhah, M. R. and Kargari, A., "The effects of aminosilane grafting on NaY zeolite-Matrimid®5218 mixed matrix membranes for CO_2/CH_4 separation", *J. Membr. Sci.*, **490**, 364 (2015).

[31] Khalilinejad, I., Sanaeepur, H. R. and Kargari, A., "Preparation of poly(ether-6-block amide)/PVC thin film composite membrane for CO_2 separation: effect of top layer thickness and operating parameters, J. Membr.", *Sci. Res.*, **1**, 124 (2015).

[32] Matteucci, S. Yampolskii, Y., Freeman, B. D. and Pinnau, I., "Transport of gases and vapors in glassy and rubbery polymers", Materials science of membranes for gas and vapor separation, Yampolskii, Y., Pinnau, I., Freeman, B. D. Eds., John Wiley & Sons Ltd., West Sussex, United Kingdom, p. 1 (2006).

[33] Rufford, T. E., Smart, S., Watson, G. C. Y., Graham, B. F., Boxall, J., Diniz da Costa, J. C. and May, E. F., "The removal of CO_2 and N_2 from natural gas: A review of conventional and emerging process technologies", *J. Petrol. Sci. Eng.*, **94-95**, 123 (2012).

[34] Kim, S., Marand, E., Ida, J. and Guliants, V. V., "Polysulfone and mesoporous molecular sieve MCM-48 mixed matrix membranes for gas separation", *Chem. Mater.*, **18**, 1149 (2006).

[35] Kargari, A. and Sanaeepur, H. R., "Application of membrane gas separation processes in petroleum industry", Advances in petroleum engineering, Sinha, S., Pant, K. K. Eds., Studium Press LLC, Houston, USA, p. 592 (2015).

[36] Sanaeepur, H. R., Kargari, A. and Nasernejad, B., "Aminosilane-functionalization of a nanoporous Y-type zeolite for application in a cellulose acetate based mixed matrix membrane for CO_2 separation", *RSC Adv.*, **4**, 63966 (2014).

[37] Sanaeepur, H. R., Kargari, A., Nasernejad, B., Ebadi Amooghin, A. and Omidkhah, M. R., "A novel Co^{2+} exchanged zeolite Y/cellulose acetate mixed matrix membrane for CO_2/N_2 separation", *J. Taiwan Inst. Chem. Eng.*, **60**, 403 (2016).

[38] Ebadi Amooghin, A., Omidkhah, M. R., Sanaeepur, H. R. and Kargari, A., "Preparation and characterization of Ag^{+}

ion-exchanged zeolite-Matrimid®5218 mixed matrix membrane for CO_2/CH_4 separation", *J. Energy Chem.*, **25**, 450 (2016).

[39] Sanaeepur, H. R., Nasernejad, B. and Kargari, A., "Cellulose acetate/nano-porous zeolite mixed matrix membrane for CO_2 separation", *Greenh. Gases Sci. Technol.*, **5**, 291 (2015).

[40] Ebadi Amooghin, A., Sanaeepur, H. R., Omidkhah, M. R. and Kargari, A., ""Ship-in-a-bottle", a new synthesis strategy for preparing novel hybrid host-guest nanocomposites for highly selective membrane gas separation", *J. Mater. Chem. A.*, **6**, 1751 (2018).

[41] Houde, A. Y., Krishnakumar, B., Charati, S. G. and Stern, S. A., "Permeability of dense (homogeneous) cellulose acetate membranes to methane, carbon dioxide, and their mixtures at elevated pressures", *J. Appl. Polym. Sci.*, **62**, 2181 (1996).

[42] Bos, A., Pünt, I. G. M., Wessling, M. and Strathmann, H., "CO_2-induced plasticization phenomena in glassy polymers", *J. Membr. Sci.*, **155**, 67 (1999).

[43] Vinit, J., Noel, C. and Monnerie, L., "Physicochemical processes occurring during the formation of cellulose diacetate membranes, research of criteria for optimizing membrane performance, II: influence of cellulose diacetate chain hydrogen on the effect of heat transfer", *Desalination*, **15**, 267 (1974).

[44] Khalilinejad, I., Kargari, A. and Sanaeepur, H. R., "Preparation and characterization of (Pebax 1657+silica nanoparticle)/PVC mixed matrix composite membrane for CO_2/N_2 separation", *Chem. Pap.*, **71**, 803 (2017).

[45] Ebadi Amooghin, A., Sanaeepur, H. R., Kargari, A. and Moghadassi, A., "Direct determination of concentration-dependent diffusion coefficient in polymeric membranes based on the Frisch method", *Sep. Purif. Technol.*, **82**, 102 (2011).

[46] Sanaeepur, H. R., Ebadi Amooghin, A., Moghadassi, A., Kargari, A., Moradi, S. and Ghanbari, D., "A novel acrylonitrile-butadiene-styrene/poly(ethylene glycol) membrane: preparation, characterization, and gas permeation study", *Polym. Adv. Technol.*, **23**, 1207 (2012).

[47] Sanaeepur, H. R., Ebadi Amooghin, A., Moghadassi, A. and Kargari, A., "Preparation and characterization of acrylonitrile–butadiene–styrene/ poly(vinyl acetate) membrane for CO_2 removal", *Sep. Purif. Technol.*, **80**, 499 (2011).

[48] Ebadi Amooghin, A., Omidkhah, M. R. and Kargari, A., "Enhanced CO_2 transport properties of membranes by embedding nano-porous zeolite particles into Matrimid®5218 matrix", *RSC Adv.*, **5**, 8552 (2015).

[49] García, A., López, C. M., García, L. V., Casanova, J. and Goldwasser, M. R., "Improvements in the synthesis of zeolites with low Si/Al ratio from Venezuelan sodium silicate, for an environmentally friendly process", *Ing. Invest.*, **36**, 62 (2016).

[50] Flanigen, E. M., Broach, R. W. and Wilson, S. T., "Introduction", Zeolites in industrial separation and catalysis, Kulprathipanja, S. Ed., WILEY-VCH Verlag GmbH & Co. KGaA, Weinheim, , p. 1 (2010).

[51] Sohn, J. R., DeCanio, S. J., Lunsford, J. H. and O'Donnell, D. J., "Determination of framework aluminium content in dealuminated Y-type zeolites: A

comparison based on unit cell size and wavenumber of i.r. bands", *Zeolites*, **6**, 225 (1986).

[52] Song, H., Jiang, B. -L., Song, H. -L. Jin, Z. -S. and Sun, X. -L., "Preparation of AgY zeolite and study on its adsorption equilibrium and kinetics", *Res. Chem. Intermed.*, **41**, 3837 (2015).

[53] Góra-Marek, K., Tarach, K. A., Piwowarska, Z., Łaniecki, M. and Chmielarz, L., "Ag-loaded zeolites Y and USY as catalysts for selective ammonia oxidation", *Catal. Sci. Technol.*, **6**, 1651 (2016).

[54] Lari, G. M., Puértolas, B., Frei, M. S., Mondelli, C. and Pérez-Ramírez, J., "Hierarchical NaY zeolites for lactic acid dehydration to acrylic acid", *Chem. Cat. Chem.*, **8**, 1507 (2016).

[55] Lemos, S. S., Deflon, V. M., Bessler, K. E. and Abbott, M. P., "Mononuclear and mixed-metal copper(I)-silver(I) complexes containing 2,2′-bibenzimidazole and triphenylphosphane as ligands: Crystal structures of $[Cu(tmbbimH_2)(PPh_3)_2](MeCOO).0.2C_7H_8$ and $[Ag_{0.55}Cu_{1.45}(\mu\text{-}bbim)(PPh_3)_4].4CH_2Cl_2$", *Transit. Metal Chem.*, **29**, 46 (2004).

[56] Johan, E., Yamauchi, Y., Matsue, N., Itagaki, Y. and Hiromichi, A., "Preparation of rare-earth-free luminescent material from partially Ag^+-exchanged zeolite X", *J. Ceram Soc. JPN*, **124**, 70 (2016).

[57] Kolobova, E., Pestryakov, A., Shemeryankina, A., Kotolevich, Y., Martynyuk, O., Tiznado Vazquez, H. J. and Bogdanchikova, N., "Formation of silver active states in Ag/ZSM-5 catalysts for CO oxidation", *Fuel*, **138**, 65 (2014).

[58] Kolobova, E., Pestryakov, A., Mamontov, G., Kotolevich, Y., Bogdanchikova, N., Farias, M., Vosmerikov, A., Vosmerikova, L. and Cortes Corberan, V., "Low-temperature CO oxidation on Ag/ZSM-5 catalysts: Influence of Si/Al ratio and redox pretreatments on formation of silver active sites", *Fuel*, **188**, 121 (2017).

[59] Zaarour, M., El Roz, M., Dong, B., Retoux, R., Aad, R., Cardin, J., Dufour, C., Gourbilleau, F., Gilson, J. -P. and Mintova, S., "Photochemical preparation of silver nanoparticles supported on zeolite crystals", *Langmuir*, **30**, 6250 (2014).

[60] Popovych, N., Kyriienko, P., Soloviev, S., Baran, R., Millotc, Y. and Dzwigaj, S., "Identification of the silver state in the framework of Ag-containing zeolite by XRD, FTIR, photoluminescence, ^{109}Ag NMR, EPR, DR UV-vis, TEM and XPS investigations", *Phys. Chem. Chem. Phys.*, **18**, 29458 (2016).

[61] Coutino-Gonzalez, E., Roeffaers, M. B. J., Dieu, B., De Cremer, G., Leyre, S., Hanselaer, P., Fyen, W., Sels, B. and Hofkens, J., "Determination and optimization of the luminescence external quantum efficiency of silver-clusters zeolite composites", *J. phys. Chem. C.*, **117**, 6998 (2013).

[62] Gachard, E., Belloni, J. and Subramanian, M. A., "Optical and EPR spectroscopic studies of silver clusters in Ag,Na-Y zeolite by y-irradiation", *J. Mater. Chem.*, **6**, 867 (1996).

[63] Schoonheydt, R. A. and Leeman, H., "Formation of the Ag_6^{x+} cluster in zeolite A.", *J. Phys. Chem.*, **93**, 2048 (1989).

[64] Gurin, V. S., Bogdanchikova, N. E. and Petranovskii, V. P., "Self-assembling of silver and copper small clusters within the

zeolite cavities: Prediction of geometry", *Mat. Sci. Eng. C.*, **18**, 37 (2001).

[65] Salavati-Niasari, M., Ganjali, M. R. and Norouzi, P., "Host (nanocavity of zeolite Y)/guest (Co(II), Ni(II) and Cu(II) complexes of unsaturated 16-membered octaaza; 3,4,11,12-tetramethyl-1,2,5,6,9,10,13,14-octaazacyclohexadecane; Me_4[16]aneN_8 nanocomposite materials (HGNM): Template synthesis, characterization and catalytic oxidation of benzyl alcohol", *Transit. Metal Chem.*, **32**, 1 (2007).

[66] Salavati-Niasari, M. and Bazarganipour, M., "Host (nanodimensional pores of zeolite Y)–guest (tetraaza[14]annulene nickel(II) complexes, [Ni(Me4R2Bzo[14]tetraeneN4)]) nanocomposite materials: "Ship-in-a-bottle" synthesis, characterization and liquid phase oxidation of phenol with hydrogen peroxide", *Catal. Commun.*, **7**, 336 (2006).

[67] Ichikawa, M., Kimura, T. and Fukuoka, A., ""Ship-in-a-bottle" synthesis of sterically crowded Fe-phthalocyanines in NaY zeolite hosts and their catalytic behavior in regioselective oxidation of alkanes", *Stud. Surf. Sci. Catal.*, **60**, 335 (1991).

[68] Li, J. -H., Chi, Z. -Q. and Chen, H. -F., "Synthesis of NaY zeolite molecular sieves from calcined diatomite", *Adv. Mater. Res.*, **236-238**, 362 (2011).

[69] Kariduraganavar, M. Y., Kittur, A. A., Kulkarni, S. S. and Ramesh, K., "Development of novel pervaporation membranes for the separation of water-isopropanol mixtures using sodium alginate and NaY zeolite", *J. Membr. Sci.*, **238**, 165 (2004).

[70] Noiroj, K., Intarapong, P., Luengnaruemitchai, A. and Jai-In, S., "A comparative study of KOH/Al_2O_3 and KOH/NaY catalysts for biodiesel production via transesterification from palm oil", *Renew. Energ.*, **34**, 1145 (2009).

[71] Oliveira, M. L. M., Miranda, A. A. L., Barbosa, C. M. B. M., Cavalcante, C. L., Azevedo, D. C. S. and Rodriguez-Castellon, E., "Adsorption of thiophene and toluene on NaY zeolites exchanged with Ag(I), Ni(II) and Zn(II)", *Fuel*, **88**, 1885 (2009).

[72] Salavati-Niasari, M., Salimi, Z., Bazarganipour, M. and Davar, F., "Synthesis, characterization and catalytic oxidation of cyclohexane using a novel host (zeolite-Y)/guest (binuclear transition metal complexes) nanocomposite materials", *Inorg. Chem. Acta*, **362**, 3715 (2009).

[73] Golubeva, O. Y., Ternovaya, N. Y., Maltseva, N. V. and Meyerstein, D., "Catalytic hydrogen oxidation using zeolite RHO modified by silver nanoparticles", *Glass Phys. Chem.*, **38**, 455 (2012).

[74] Zhou, T., Luo, L., Hu, S., Wang, S., Zhang, R., Wu, H., Jiang, Z., Wang, B. and Yang, J., "Janus composite nanoparticle-incorporated mixed matrix membranes for CO_2 separation", *J. Membr. Sci.*, **489**, 1 (2015).

[75] Manna, A., Imae, T., Iida, M. and Hisamatsu, N., "Formation of silver nanoparticles from a N-hexadecylethylenediamine silver nitrate complex", *Langmuir*, **17**, 6000 (2001).

[76] Rindfleisch, F., DiNoia, T. P. and McHugh, M. A., "Solubility of polymers and copolymers in supercritical CO_2", *J. Phys. Chem.*, **100**, 15581 (1996).

[77] Ebadi Amooghin, A., Sanaeepur, H. R., Moghadassi, A., Kargari, A., Ghanbari, D. and Sheikhi Mehrabadi, Z., "Modification of ABS membrane by PEG for capturing carbon dioxide from CO_2/N_2 streams", *Sep. Sci. Technol.*, **45**, 1385 (2010).

[78] Zamiri, M. A., Kargari, A. and Sanaeepur, H. R., "Ethylene vinyl acetate/poly(ethylene glycol) blend membranes for CO_2/N_2 separation", *Greenh. Gases Sci. Technol.*, **5**, 668 (2015).

[79] D'Alessandro, D. M., Smit, B. and Long, J. R., "Carbon dioxide capture: prospects for new materials", *Angew. Chem. Int. Edit.*, **49**, 6058 (2010).

[80] Liu, J., Hou, X., Park, H. B. and Lin, H., "High-performance polymers for membrane CO_2/N_2 separation", *Chem. Eur. J.*, **22**, 1 (2016).

[81] Kim, S. J., Jeon, H., Kim, D. J. and Kim, J. H., "High-performance polymer membranes with multifunctional amphiphilic micelles for CO_2 capture", *Chem. Sus. Chem.*, **8**, 3783 (2015).

[82] Lee, M. S., Park, M., Kim, H. Y. and Park, S. J., "Effects of microporosity and surface chemistry on separation performances of N-containing pitch-based activated carbons for CO_2/N_2 binary mixture", *Sci. Rep.*, **6**, 23224 (2016).

[83] Lin, H., "Solubility selective membrane materials for carbon dioxide removal from mixtures with light gases", The University of Texas at Austin, Ph.D. Thesis, (2005).

[84] Robeson, L. M., Smith, Z. P., Freeman, B. D. and Paul, D. R., "Contributions of diffusion and solubility selectivity to the upper bound analysis for glassy gas separation membranes", *J. Membr. Sci.*, **453**, 71 (2014).

[85] Peng, F., Lu, L., Sun, H., Wang, Y., Liu, J. and Jiang, Z., "Hybrid organic-inorganic membrane: Solving the tradeoff between permeability and selectivity", *Chem. Mater.*, **17**, 6790 (2005).

[86] Ghasemi Estahbanati, E., Omidkhah, M. R. and Ebadi Amooghin, A., "Interfacial design of ternary mixed matrix membranes containing Pebax 1657/silver-nanopowder/[BMIM][BF_4] for improved CO_2 separation performance", *ACS Appl. Mater. Interfaces*, **9**, 10094 (2017).

[87] Bettens, B., Dekeyzer, S., Van der Bruggen, B., Degrève, J. and Vandecasteele, C., "Transport of pure components in pervaporation through a microporous silica membrane", *J. Phys. Chem. B.*, **109**, 5216 (2005).

[88] Yu, Y., Mai, J., Huang, L., Wang, L. and Li, X., ""Ship-in-a-bottle" synthesis of ionic liquids in NaY supercages for CO_2 capture", *RSC Adv.*, **4**, 12756 (2014).

[89] Kassaee, M. H., Sholl, D. S. and Nair, S., "Preparation and gas adsorption characteristics of zeolite MFI crystals with organic-functionalized interiors", *J. Phys. Chem. C.*, **115**, 19640 (2011).

[90] Hasegawa, Y., Tanaka, T., Watanabe, K., Jeong, B. -H., Kusakabe, K. and Morooka, S., "Separation of CO_2-CH_4 and CO_2-N_2 systems using ion-exchanged zeolite membranes with different Si/Al ratios", *Korean J. Chem. Eng.*, **19**, 309 (2002).

[91] Bastani, D., Esmaeili, N. and Asadollahi, M., "Polymeric mixed matrix membranes containing zeolites as a filler for gas separation applications: A review", *J. Ind. Eng. Chem.*, **19**, 375 (2013).

[92] Alavi, S. A., Kargari, A., Sanaeepur, H. R.

and Karimi, M., "Preparation and characterization of PDMS/zeolite 4A/PAN mixed matrix thin film composite membrane for CO_2/N_2 and CO_2/CH_4 separations", *Res. Chem. Intermed.*, **43**, 2959 (2017).

[93] Sanders, D. F., Smith, Z. P., Guo, R., Robeson, L. M., McGrath, J. E., Paul, D. R. and Freeman, B. D., "Energy-efficient polymeric gas separation membranes for a sustainable future: A review", *Polymer*, **54**, 4729 (2013).

[94] Mubashir, M., Fong, Y. Y., Leng, C. T. and Keong, L. K., "Optimization of spinning parameters on the fabrication of NH2-MIL-53(Al)/cellulose acetate (CA) hollow fiber mixed matrix membrane for CO_2 separation", *Sep. Purif. Technol.*, **215**, 32 (2019).

[95] Mubashir, M., Fong, Y. Y., Keong, L. K., Leng, C. T. and Jusoh, N., "Efficient CO_2/N_2 and CO_2/CH_4 separation using NH_2-MIL-53(Al)/cellulose acetate (CA) mixed matrix membranes", *Sep. Purif. Technol.*, **199**, 140 (2018).

[96] Kim, W. -G., Lee, J. S., Bucknall, D. G., Koros, W. J. and Nair, S., "Nanoporous layered silicate AMH-3/cellulose acetate nanocomposite membranes for gas separations", *J. Membr. Sci.*, **441**, 129 (2013).

[97] Ahmad, A. L., Jawad, Z. A., Low, S. C. and Zein, S. H. S., "A cellulose acetate/multi-walled carbon nanotube mixed matrix membrane for CO_2/N_2 separation", *J. Membr. Sci.*, **451**, 55 (2014).